Lithium-Ion Batteries Hot Paper

Deutsche Ausgabe: DOI: 10.1002/ange.201608146
Internationale Ausgabe: DOI: 10.1002/anie.201608146

Mesoporous Amorphous Silicon: A Simple Synthesis of a High-Rate and Long-Life Anode Material for Lithium-Ion Batteries

*Liangdong Lin, Xuena Xu, Chenxiao Chu, Muhammad K. Majeed, and Jian Yang**

Abstract: *Amorphous Si (a-Si) shows potential advantages over crystalline Si (c-Si) in lithium-ion batteries, owing to its high lithiation potential and good tolerance to intrinsic strain/stress. Herein, porous a-Si has been synthesized by a simple process, without the uses of dangerous or expensive reagents, sophisticated equipment, and strong acids that potential cause environment risks. These porous a-Si particles exhibit excellent electrochemical performances, owing to their porous structure, amorphous nature, and surface modification. They deliver a capacity of 1025 mAh g^{-1} at 3 A g^{-1} after 700 cycles. Moreover, the reversible capacity after electrochemical activation, is quite stable throughout the cycling, resulting in a capacity retention about around 88 %. The direct comparison between a-Si and c-Si anodes clearly supports the advantages of a-Si in lithium-ion batteries.*

Silicon has been regarded as one of the promising next-generation anode materials for rechargeable lithium-ion batteries (LIBs),[1] owing to its high theoretical capacity (ca. 3579 mAh g^{-1}), almost ten-times higher than that of graphite (ca. 372 mAh g^{-1}). Its high abundance on earth and the low toxicity strengthen the position of silicon over the other candidates. But silicon shows massive volume expansion upon cycling, which easily results in structure failure, poor capacity retention, and inferior coulombic efficiency. These issues greatly hinder the practical applications of silicon. To tackle these tough issues, many strategies have been developed, such as structure engineering (porous/hollow structure),[2] size/shape control (nanowires, nanotubes),[3] surface modification (carbon or MO_x coating),[4] and component modulation (M-Si alloy).[5] Although these efforts have achieved remarkable progresses, they still do not meet all the requirements for Si. So, it is necessary to search other ways for making high-performance silicon anodes.

Because silicon eventually becomes amorphous during electrochemical lithiation/delithiation, the attempt to use amorphous silicon (a-Si) as an anode from the beginning draws intense interest. Moreover, a-Si possesses several advantages over crystalline Si (c-Si). Firstly, a-Si has high resistance to structure fracture.[6] This property is attributed to isotropic strain/stress in a-Si, which restrains the particle pulverization and keeps the structure stable. This stability is extremely important in the electrochemical performance of silicon as an anode. Secondly, a-Si reacts with lithium at a relatively higher potential (ca. 0.22 V) than c-Si (0.12 V).[7] This fact offers us the basis to increase the cut-off potential during the lithiation, which not only inhibits the formation of lithium dendrites and improves the battery safety, but also reduces the volume change and increases the cycling life. However, previous studies about using a-Si as an anode material are quite limited, because of the difficulties in chemical synthesis and structure engineering. The reported syntheses of a-Si always involve expensive and dangerous reagents, such as NaK alloy, silanes,[3a,8] or sophisticated equipment such as e-beam evaporation,[9] radio-frequency magnetron sputtering,[10] both of which greatly limit the exploration on a-Si as an anode material. Thus, fabricating a-Si by a simple method without the above drawbacks, is a great challenge. On the other hand, most of the as-obtained a-Si anodes are either thin films or solid particles.[8–11] To our knowledge, no porous a-Si has been explored as the anode before, although porous structures have been demonstrated to be very helpful in crystalline Si (c-Si).[4a]

Herein, porous a-Si powders, are synthesized by a solvothermal reaction followed by a high-temperature annealing, (Scheme 1). The solvothermal reaction between $SiCl_4$ and Mg is conducted in glyme. Using $SiCl_4$ as the silicon source, rather than silanes, could reduce the cost and risk of the reaction, allowing mass production in the future. The similar advantages apply to the reducing agent, Mg powders. They are cheap, safe, and easily accessed, compared to NaK alloy and sodium naphthanide used in other routes.[12] Most strikingly, this solvothermal reaction at 100 °C could produce elemental

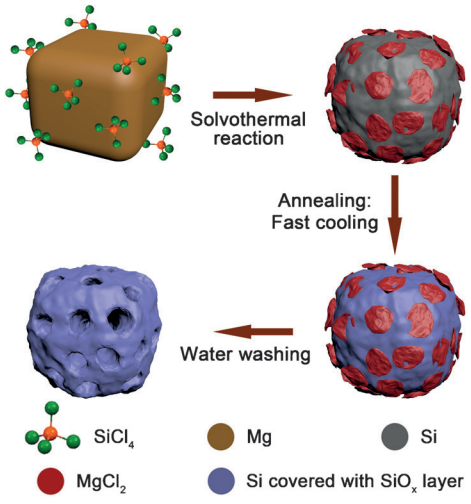

Scheme 1. Synthesis process of porous a-Si anode.

[*] L. Lin, X. Xu, C. Chu, M. K. Majeed, Prof. J. Yang
Key Laboratory of Colloid and Interface Chemistry Ministry of Education, School of Chemistry and Chemical Engineering
Shandong University
Jinan 250100 (P. R. China)
E-mail: yangjian@sdu.edu.cn

Supporting information for this article can be found under: http://dx.doi.org/10.1002/anie.201608146.

silicon (Figure S1 in the Supporting Information). Glyme is important to this reaction, because it has lone-pair electrons to solvate Mg species, and good miscibility with $SiCl_4$. These properties facilitate the reaction between Mg and $SiCl_4$ at a low temperature. During this process, many organic molecules are also encapsulated in the product (Figure S2), which increases the electrical resistances between neighboring particles. Thus, high-temperature annealing is carried out to get rid of these organics completely.

Quick cooling of the product to room temperature maintains the amorphous nature of Si, as confirmed in that only the diffraction peaks of $MgCl_2$ are observed in the XRD pattern (Figure S3). At this point, the particles are still solid (Figure S4). After washed with water and ethanol, the particles become highly porous (Figure S5), as a result of the removal of $MgCl_2$. More importantly, we do not need strong acids such as HCl and HF any more for the post-treatments, which alleviates serious environmental concerns about the disposal of these acids. The safe and cheap reagents, conventional equipment, and simple operation to give porous structured Si make the synthesis attractive.

The final product is highly porous, as shown in the SEM image (Figure 1a) and also supported by TEM images (Figure 1b) that further disclose the pore sizes are in the range 10–50 nm. It is believed that the 3D-interconnected mesopores would aid the contact between electrolyte and electrode, accommodate the volume change during lithiation/delithiation, and shorten the diffusion distance from the surface to the inside of the electrode. The consequences greatly improve the cycling stability and rate capability of this product. Selected area electron diffraction (SAED) of these porous particles (the inset of Figure 1b) is highly diffused, indicating the amorphous nature. This result is also confirmed by the absences of lattice fringes in the HRTEM image (Figure 1c) and diffraction peaks in the XRD pattern (Figure S6). This amorphous nature means that the strain/stress caused by lithiation/delithiation is homogeneous, effectively inhibiting the particle pulverization and enhancing the structure stability. EDS spectra (Figure S7) shows that these porous amorphous particles are made of silicon and oxygen with an atomic ratio of 79.1:20.9. The presence of oxygen in the particles is inevitable, because some post-treatments such as the particle filtration, were conducted in air. Even the drying in vacuum and the annealing in Ar could not completely exclude oxygen. Furthermore, this surface oxidation could easily happen at room temperature during the storage, indicated by an apparent change in color (Figure S8a). Once SiO_x is formed on the surface after annealing, it would prevent the particles from being further oxidized (Figure S8b). Although the formation of SiO_x lowers the initial coulombic efficiency and increases the electron resistance, it also improves the structure stability, which has been demonstrated by Cui et al. for Si@SiO_x nanotubes.[3b] Element mapping shows that silicon and oxygen are uniformly dispersed throughout the particle (Figure 1d), consistent with the surface oxidation. For the sake of clarity, porous a-Si particles are denoted as p/a-Si from now on.

The porous structure, amorphous nature, and surface oxidation of p/a-Si are further investigated by nitrogen sorption isotherm, Raman spectrum, and XPS spectrum. As shown in Figure 2a, there is a small hysteresis at the high pressure in nitrogen sorption isotherms of p/a-Si, indicating the porous structure in the product. On the basis of BET theory, the pore size distribution could be obtained (Figure 2b). Most of the pores have their sizes ranging from 10–50 nm, consistent with the result from TEM images. The amorphous nature of p/a-Si is confirmed by Raman spectrum (Figure 2c), where the characteristic peak of a-Si at 480 cm^{-1} could be easily observed.[13] Moreover, there is no sign of the peaks from carbon materials between 1300–1600 cm^{-1} (Figure S9), excluding the presence of a carbon coating caused by the decomposition of organic molecules at a high temperature. XPS spectra are employed to disclose the surface status of p/a-Si. Three peaks could be derived from the high-resolution XPS spectrum of Si 2p (Figure 2d). The peak at 99.8 eV arises from elemental silicon, and those at 102.5 and 103.7 eV come from Si^{2+} and Si^{4+}.[14] The ratio of Si^0: Si^{2+}: Si^{4+}

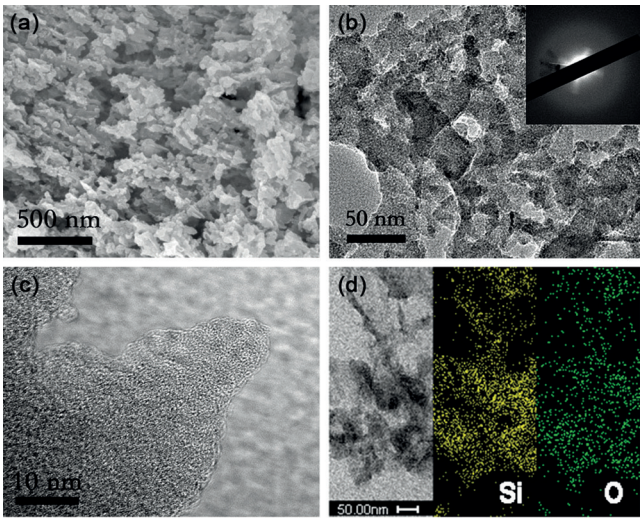

Figure 1. a) SEM image, b) TEM image, inset: SAED pattern, c) HRTEM image, and d) element mapping of p/a-Si.

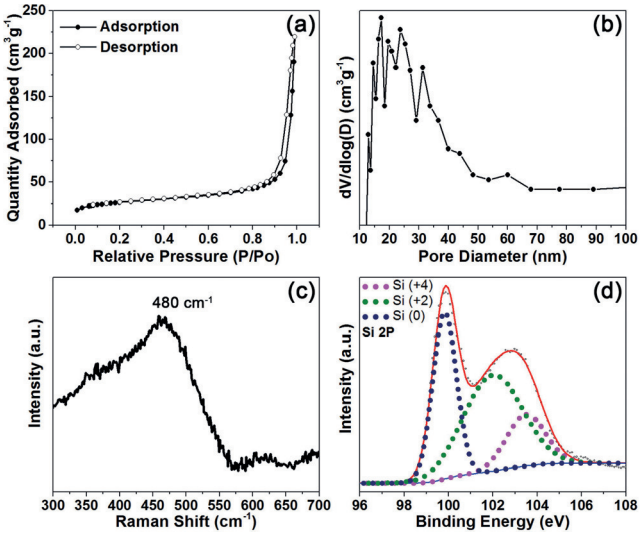

Figure 2. a) Nitrogen adsorption–desorption isotherms, b) pore size distribution, c) Raman spectrum, and d) XPS spectrum of p/a-Si.

is 34.1 %: 48.6 %: 17.3 %, indicating the majority of Si atoms on the surface are oxidized. After Ar-ion sputtering, the content of elemental silicon increases greatly (Figure S10), confirming the surface oxidation.

The electrochemical performances of p/a-Si as an anode material for LIBs, are summarized in Figure 3. Figure 3a shows the discharge–charge profiles at a current density of 500 mA g^{-1} over a voltage window of 0.001–1.5 V for the first three cycles. There are several inconspicuous plateaus for the first discharge process. The first one at 0.65 V is likely to come from the formation of the solid-electrolyte interphase (SEI) film.[15] It disappears in the subsequent cycles, consistent with the irreversibility of this reaction. The second one in the voltage range from 0.50 to 0.25 V, originates from the reduction of SiO_x at the surface.[16] The distinctive discharge plateau at 0.1 V caused by the lithium alloying of crystalline silicon,[17] is not observed in our case. But a slope below 0.25 V is present instead, which is in good agreement with the behaviors of amorphous silicon in the rest cycles. Although the discharge capacity is as high as 2599 mAh g^{-1}, only a reversible capacity of 1679 mAh g^{-1} is obtained for the first charge process, resulting in a coulombic efficiency of 64.6 %. The low initial coulombic efficiency indicates that there are irreversible reactions in the first cycle, such as the reduction of SiO_x and the formation of the SEI film. In spite of this, the coulombic efficiency quickly increases to 92.9 % at the second cycle, and approaches to 95.7 % at the third cycle. After the first cycle, the discharge and charge profiles in the following cycles basically overlap with each other, suggesting the good electrochemical reversibility.

Figure 3b shows the rate performance of p/a-Si. As the current density increases from 1 A g^{-1} to 2, 3, and 5 A g^{-1}, p/a-Si gives a capacity of 1608, 1387, 1180, and 781 mAh g^{-1}. If the current density goes back to 1 A g^{-1}, the capacity could be recovered as 1580 mAh g^{-1}, confirming the excellent stability. The continuous cycling of p/a-Si at 1 A g^{-1} for 100 cycles, does not show an obvious capacity loss, and ends at a capacity of 1577 mAh g^{-1} (Figure 3c). In view of the mass loading at approximately 0.8 mg cm^{-2} in our case, the areal capacity could reach 1.24 mAh cm^{-2}, which is much better than many previous reports on Si (Figure 3d).[2b,c,3b,8a,10,11] For example, a-Si grown on Cu nano-pillars showed a high specific capacity of 1627 mAh g^{-1} after 100 cycles at 1 A g^{-1},[8a] but its areal capacity was only about 0.150 mAh cm^{-2}, due to the small mass loading of 0.092 mg cm^{-2}. A similar result was also reported for an alumina-coated a-Si pattern that was prepared by photolithography followed with reactive ion etching.[10] Although such an alumina coating kept the capacity of a-Si stabilized at around 2800 mAh g^{-1} after 40 cycles at 3.75 A g^{-1}, the areal capacity was about 0.065 mAh cm^{-2}, because the mass loading is only about 0.023 mg cm^{-2}. More importantly, the syntheses of these composites involved expensive and explosive SiH_4, sophisticated radio-frequency magnetron sputtering, and laborious methods such as optical photolithography, all of which have been avoided in our case. The long-term cycling of p/a-Si at a high rate is conducted, as shown in Figure 3e. The p/a-Si anode is electrochemically activated at 500 mA g^{-1} for the first ten cycles, and then cycled at a current density of 3 A g^{-1}. After 700 cycles, the reversible capacity remains at 1025 mAh g^{-1}, indicating that p/a-Si decays only 0.016 % per cycle from 11th to 700th cycle. This good cycling stability is confirmed from p/a-Si obtained from independent synthesis (Figure S11), suggesting its good reproducibility. All these results are obtained without carbon coating. If p/a-Si can be covered by carbon properly, the electrochemical performances would be further improved.

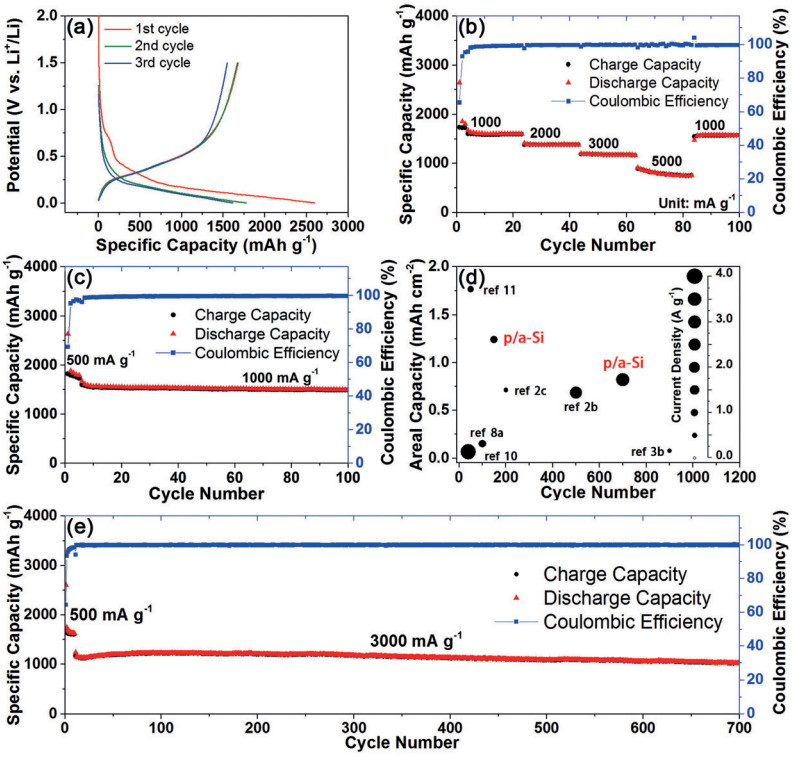

Figure 3. Electrochemical characteristics of p/a-Si. a) Voltage profiles of p/a-Si for the first three cycles. b) Rate performance and coulombic efficiency of p/a-Si at different current densities. c) Cycling performance and coulombic efficiency of p/a-Si at 1000 mA g^{-1}. d) Electrochemical performances of p/a-Si and many previous reports on silicon. e) Cycling performance and coulombic efficiency of p/a-Si at a current density of 3000 mA g^{-1}.

To illustrate the advantages of the amorphous nature, a similar structure containing crystalline Si, denoted as p/c-Si, was prepared by slow cooling of the product to room temperature after annealing. This control is vital to the crystallization of Si, because it gives enough time for silicon atoms to move to form a periodic structure. Otherwise, the atoms would be frozen at the sites where they are produced, resulting in a disordered structure. The formation of crystalline Si is confirmed by the XRD pattern, Raman spectrum, and the lattice fringes in the HRTEM image (Figure S12). Meanwhile, the porous structure is also maintained for p/c-Si. With these features in common the results obtained by the comparison between p/a-Si and p/c-Si are reliable. The rate measurements indicate that p/c-Si degrades much faster at high

rates than p/a-Si (Figure S13a), indicating the superior charge-transfer kinetics in p/a-Si. This result is also supported by EIS spectra (Figure S13b), in which the charge-transfer resistance derived from the depressed semicircle at the high-to-medium frequencies, is much smaller in p/a-Si than that in p/c-Si. This result suggests superior diffusion kinetics in p/a-Si.

Overall, the excellent performances of p/a-Si in cycling stability and rate capability could be attributed to the synergistic effect of porous structure, amorphous nature, and surface modification. As discussed above, the porous structure increases the specific surface area, reduces the areal current density, and then lowers the electrode polarization. It also benefits the penetration of electrolyte into the electrode, and shortens the diffusion distance of lithium ions. Most important, it contains a large quantity of empty spaces, allows the structure breathe upon cycling, and keeps the structure stable (Figure S14). The amorphous nature has a similar effect on the structure. Because it facilitates the isotropic strain/stress during the lithiation/delithiation process, this would enhance the structure stability. The effect of surface modification of p/a-Si by SiO_x is similar but in a different way. All these results suggest that the structure stability is important to the cycling.

In summary, porous a-Si particles are synthesized by a solvothermal reaction followed with a high-temperature annealing. This process did not involve expensive or dangerous reagents, sophisticated equipment, or strong acids for post-treatment, making it very attractive for the mass production in the future. Although the surface is partially oxidized as a result of exposure to air, porous a-Si particles still exhibit excellent electrochemical performances, because the porous structure, amorphous nature, and SiO_x coating greatly stabilize the structure, and promote the charge transportation. After 700 cycles at $3\,A\,g^{-1}$, these particles deliver a capacity of $1025\,mAh\,g^{-1}$, corresponding to a capacity retention of 88% relative to that after electrochemical activation at a low current density. The areal capacity could be as high as $1.24\,mAh\,cm^{-2}$, even without carbon. All these results indicate the promising potential of porous a-Si powders.

Acknowledgements

This work was supported by the 973 Project of China (No. 2011CB935901), the National Nature Science Foundation of China (Nos. 51172076, 21471090, and 61527809), Shandong Provincial Natural Science Foundation for Distinguished Young Scholar (JQ201205), and Taishan Scholarship in Shandong Provinces (No. Ts201511004).

Keywords: amorphous materials · anodes · lithium-ion batteries · mesoporous structures · silicon

How to cite: *Angew. Chem. Int. Ed.* **2016**, *55*, 14063–14066
Angew. Chem. **2016**, *128*, 14269–14272

[1] a) M. A. Rahman, G. Song, A. I. Bhatt, Y. C. Wong, C. Wen, *Adv. Funct. Mater.* **2016**, *26*, 647–678; b) H. Zhao, W. Yuan, G. Liu, *Nano Today* **2015**, *10*, 193–212; c) M. N. Obrovac, V. L. Chevrier, *Chem. Rev.* **2014**, *114*, 11444–11502.

[2] a) H. Kim, B. Han, J. Choo, J. Cho, *Angew. Chem.* **2008**, *120*, 10305–10308; b) X. K. Huang, J. Yang, S. Mao, J. B. Chang, P. B. Hallac, C. R. Fell, B. Metz, J. W. Jiang, P. T. Hurley, J. H. Chen, *Adv. Mater.* **2014**, *26*, 4326–4332; c) J. Liang, X. Li, Q. Cheng, Z. Hou, L. Fan, Y. C. Zhu, Y. T. Qian, *Nanoscale* **2015**, *7*, 3440–3444.

[3] a) A. M. Chockla, J. T. Harris, V. A. Akhavan, T. D. Bogart, V. C. Holmberg, C. Steinhagen, C. B. Mullins, K. J. Stevenson, B. A. Korgel, *J. Am. Chem. Soc.* **2011**, *133*, 20914–20921; b) H. Wu, G. Chan, J. W. Choi, I. Ryu, Y. Yao, M. T. McDowell, S. W. Lee, A. Jackson, Y. Yang, L. B. Hu, Y. Cui, *Nat. Nanotechnol.* **2012**, *7*, 310–315; c) J. Wang, X. C. Meng, X. L. Fan, W. B. Zhang, H. Y. Zhang, C. S. Wang, *ACS Nano* **2015**, *9*, 6576–6586.

[4] a) Y. Yu, L. Gu, C. B. Zhu, S. Tsukimoto, P. A. V. Aken, J. Maier, *Adv. Mater.* **2010**, *22*, 2247–2250; b) N. Liu, H. Wu, M. T. McDowell, Y. Yao, C. Wang, Y. Cui, *Nano Lett.* **2012**, *12*, 3315–3321; c) Y. H. Xu, Y. J. Zhu, F. D. Han, C. Luo, C. S. Wang, *Adv. Energy Mater.* **2015**, *5*, 1400753; d) W. Sun, R. Hu, M. Zhang, J. Liu, M. Zhu, *J. Power Sources* **2016**, *318*, 113–120.

[5] a) S. Chae, M. Ko, S. Park, N. Kim, J. Ma, J. Cho, *Energy Environ. Sci.* **2016**, *9*, 1251–1257; b) B. D. Polat, O. Keles, K. Amine, *Nano Lett.* **2015**, *15*, 6702–6708.

[6] a) L. Y. Beaulieua, T. D. Hatcharda, A. Bonakdarpoura, M. D. Fleis-chauera, J. R. Dahn, *J. Electrochem. Soc.* **2003**, *150*, A1457–A1464; b) J. T. Yina, M. Wadab, K. Yamamotob, Y. Kitanoa, S. Tanasea, T. Sakai, *J. Electrochem. Soc.* **2006**, *153*, A472–A477; c) M. T. McDowell, S. W. Lee, J. T. Harris, B. A. Korgel, C. M. Wang, W. D. Nix, Y. Cui, *Nano Lett.* **2013**, *13*, 758–764.

[7] L. F. Cui, R. Ruffo, C. K. Chan, H. L. Peng, Y. Cui, *Nano Lett.* **2009**, *9*, 491–495.

[8] a) G. Kim, S. Jeong, J. H. Shin, J. Cho, H. Lee, *ACS Nano* **2014**, *8*, 1907–1912; b) S. Murugesan, J. T. Harris, B. A. Korgel, K. J. Stevenson, *Chem. Mater.* **2012**, *24*, 1306–1315.

[9] H. Ghassemi, M. Au, N. Chen, P. A. Heiden, R. S. Yassar, *ACS Nano* **2011**, *5*, 7805–7811.

[10] Y. He, X. Yu, Y. Wang, H. Li, X. Huang, *Adv. Mater.* **2011**, *23*, 4938–4941.

[11] a) F. Farmakis, C. Elmasides, P. Fanz, M. Hagen, N. Georgoulas, *J. Power Sources* **2015**, *293*, 301–305; b) M. Li, J. Gu, X. Feng, H. He, C. Zeng, *Electrochim. Acta* **2015**, *164*, 163–170.

[12] a) F. Dai, J. T. Zai, R. Yi, M. L. Gordin, H. Sohn, S. R. Chen, D. H. Wang, *Nat. Commun.* **2014**, *5*, 3605; b) R. K. Baldwin, K. A. Pettigrew, J. C. Garno, P. P. Power, G. Y. Liu, S. M. Kauzlarich, *J. Am. Chem. Soc.* **2002**, *124*, 1150–1151; c) R. K. Baldwin, K. A. Pettigrew, E. Ratai, M. P. Augustine, S. M. Kauzlarich, *Chem. Commun.* **2002**, 1822–1823.

[13] E. Pollak, G. Salitra, V. Baranchugov, D. Aurbach, *J. Phys. Chem. C* **2007**, *111*, 11437–11444.

[14] Z. H. Bao, M. R. Weatherspoon, S. Shian, Y. Cai, P. D. Graham, S. M. Allan, G. Ahmad, M. B. Dickerson, B. C. Church, Z. T. Kang, H. W. Abernathy, C. J. Summers, M. L. Liu, K. H. Sandhage, *Nature* **2007**, *446*, 172–175.

[15] M. Y. Nie, D. P. Abraham, Y. J. Chen, A. Bose, B. L. Lucht, *J. Phys. Chem. C* **2013**, *117*, 13403–13412.

[16] M. T. McDowell, S. W. Lee, I. Ryu, H. Wu, W. D. Nix, J. W. Choi, Y. Cui, *Nano Lett.* **2011**, *11*, 4018–4025.

[17] N. Lin, Y. Han, L. B. Wang, J. B. Zhou, J. Zhou, Y. C. Zhu, Y. T. Qian, *Angew. Chem. Int. Ed.* **2015**, *54*, 3822–3825; *Angew. Chem.* **2015**, *127*, 3893–3896.

Received: August 20, 2016
Published online: October 6, 2016

